Journal of Alloys and Compounds 890 (2021) 161758

Contents lists available at ScienceDirect

Journal of Alloys and Compounds

journal homepage: www.elsevier.com/locate/jalcom

Chemical vapor deposition of $CoFe_2O_4$ micropillar arrays with enhanced magnetic properties

B. Aspe[a], A. Malyeyev[b], A. Vakilinejad[a], K. Menguelti[a], A. Michels[b], N. Bahlawane[a,*]

[a] Material Research and Technology Department, Luxembourg Institute of Science and Technology, Rue du Brill, L-4422 Belvaux, Luxembourg
[b] Department of Physics and Materials Science, University of Luxembourg, 162A Avenue de la Faïencerie, L-1511 Luxembourg, Luxembourg

ARTICLE INFO

Article history:
Received 31 May 2021
Received in revised form 24 August 2021
Accepted 26 August 2021
Available online 30 August 2021

Keywords:
CFO
Ferromagnetic
Micropillar
CVD
Thin films

ABSTRACT

Single-step thermal chemical vapor deposition was optimized at 400 °C for the growth of $CoFe_2O_4$ spinel thin films starting from the corresponding metal acetylacetonate precursors. Enhanced magnetization was observed for conditions leading to a columnar growth with a preferred (100) orientation. The implemented liquid precursor delivery secured a reliable films' composition control and a straightforward dosage of acetylacetone, as a molecular growth inhibitor, to enhance the film conformality on structured surfaces. The optimized conditions enabled an efficient micro-pore filling, and the fabricated ordered micropillar arrays feature a coercivity of 1.8 kOe and a saturation magnetization of 350 emu/cm^3. The implemented state-of-the-art up-scalable microfabrication technology, the reasonable thermal budget and the resulting high magnetic performance pave the way towards the development of innovative magnetoelectric devices.

1. Introduction

Ferromagnetic materials have long been of scientific interest to fulfil various functionalities in a large range of devices. Ferromagnetic materials with high coercivity are generally used as permanent magnets and in data storage [1], whereas those featuring high electromagnetic loss are relevant for microwave absorption [2]. In contrast, a high magnetic permeability and good ferromagnetic resonance properties are essential for the design of microwave devices such as antennas and tuneable filters [3,4], while magnetostriction is a key property of ferromagnetic materials destined to transduction, micro-displacement actuation, noncontact stress and torque sensing [5–9].

Among ferromagnetic materials, metal oxide thin films are appealing in terms of integration and miniaturization. In this context, an advanced control over their structural properties is a pre-requisite, especially in view of the anisotropic properties. As a ferro/ferrimagnetic oxide, $CoFe_2O_4$ (CFO) is one of the most investigated ferrites owing to its moderate magnetization (87 emu/g (455 emu/cm^3) at 300 K and for a magnetic field of 15 kOe along the c-axis on single crystal) [10], high coercivity [11], magnetostriction [12] and high Curie temperature (520 °C) as well as its good chemical stability [13]. In contrast to most ferrites, CFO exhibits a strong magnetic anisotropy [14].

Cobalt ferrite films have been prepared using various physical methods including pulsed laser deposition (PLD) [15–17] and sputtering [18,19]. Chemical vapor deposition (CVD) is an alternative technique presenting the advantage of being non-line-of-site, which enables deposition of films on three-dimensional structures. Furthermore, CVD is appealing for depositions on large substrates at moderate temperatures [20,21].

Prepared films usually present defects in the lattice, at the surface and grain boundaries, which impact the magnetic properties. Post-deposition annealing is accepted as a promising solution to improve and control the structural properties of CFO [18]. Indeed, heat treatments can heal defects in the crystalline structure [22] and grain boundaries [23]. The heat treatment at 750 °C under magnetic field (0.5 T) enables the alignment of the initially random easy axis, < 100 > , along the field direction, which increases the magnetic anisotropy [24]. The grain orientation under magnetic field (2 T) prior to sintering at 1350 °C yields a < 100 > preferred orientation and an ensuing increase of the magnetostriction up to −270 ppm [9]. The thermal budget associated to the magnetic annealing might however become a limitation for device manufacturing, which favours growth methods enabling a direct crystalline orientation. In this context, a significantly enhanced out-of-plane magnetization (190 emu/cm^3) and coercivity (3.8 kOe) were observed for the compressively strained epitaxial CFO < 400 > on (100)$SrTiO_3$ relative

* Correspondence to: Luxembourg Institute of Science and Technology (LIST), Materials Research and Technology Department, 41, rue du Brill, L-4422 Belvaux, Luxembourg
E-mail address: naoufal.bahlawane@list.lu (N. Bahlawane).

https://doi.org/10.1016/j.jallcom.2021.161758
0925-8388/

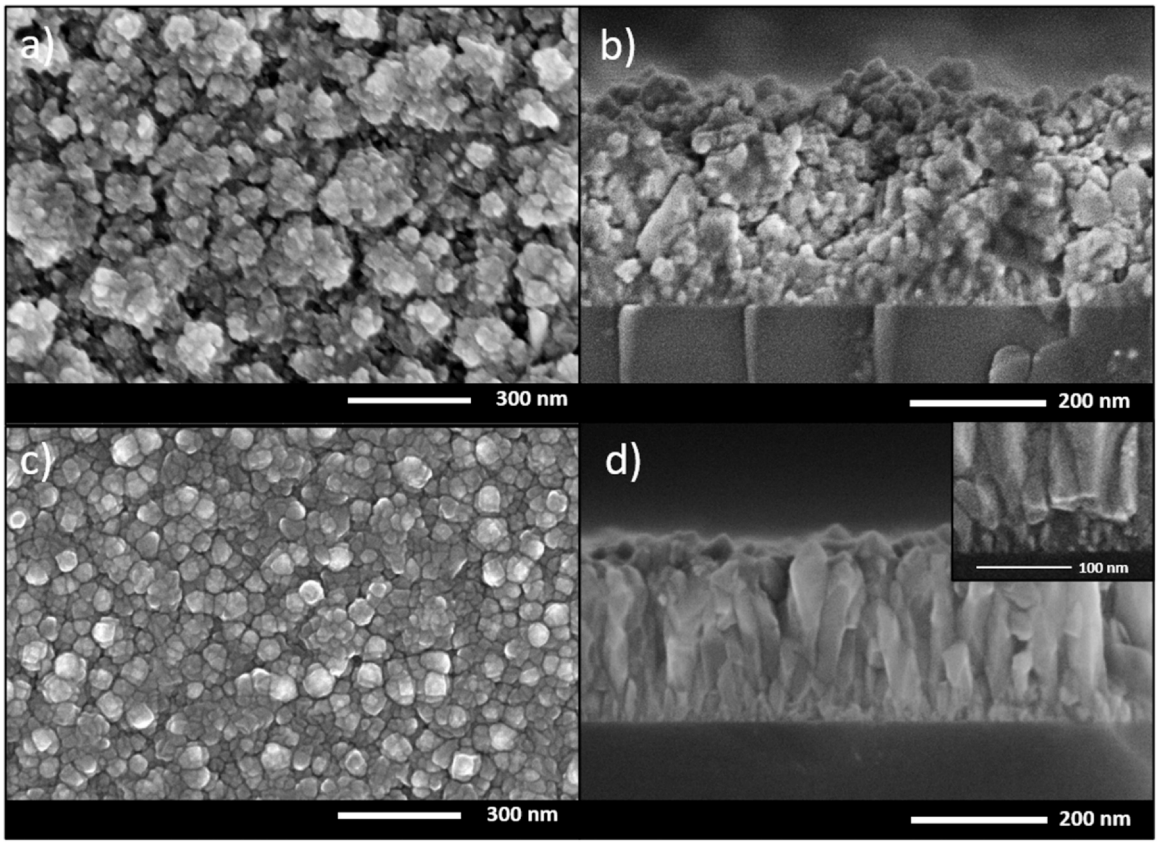

Fig. 1. (a, c) Top view and (b, d) cross-section scanning electron micrographs of CFO_90 and CFO_30.

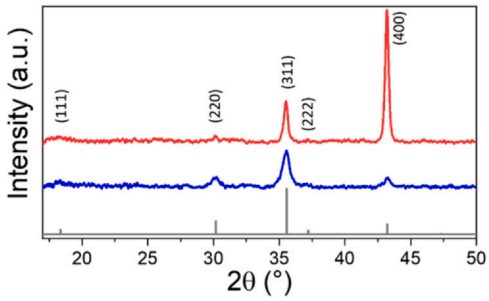

Fig. 2. Θ-2θ X-ray diffraction patterns of CFO_30 (red), CFO_90 (blue) and CoFe2O4 powder.
Retrieved from the database JCPDS file #04-006-4148 [36].

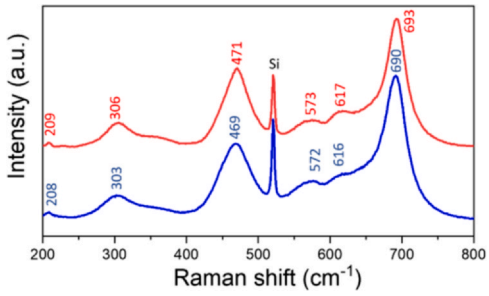

Fig. 3. Raman spectra of CFO_30 (red) and CFO_90 (blue).

to the tensile strained counterpart on (001)MgO [25]. The use of $SrTiO_3$ is however not systematically compatible with devices functionality, and it is associated with an inherent increase of the cost.

$CoFe_2O_4$ has widely been investigated for the design of multiferroic composites, where the magnetoelectric (ME) coupling is mediated by its magnetostriction that was evaluated as λ_{100} = −885 ppm for $Co_{0.8}Fe_{2.2}O_4$ [12] and $CoFe_2O_4$ [26]. Various architectures were adopted for the design of multiferroic composites, including self-assembly [27–31], and sacrificial templating approaches [32,33]. High ME coupling is expected from embedded one-dimensional magnetic nano- or microstructures in a ferroelectric matrix [27,28,34], an architecture that is challenged by the difficulty encountered for the high-aspect ratio processing of CFO. This challenge is addressed in the present study using a robust and reliable approach at moderate temperature using chemical vapor deposition and conventional microfabrication processes. Attention is given to the magnetic properties, such as the saturation magnetization, coercivity and related magnetic anisotropy, which reach relevant performances for future multiferroic composites fabrication.

2. Experimental methods

CFO thin films were grown on < 100 > silicon substrate (Siegert Wafer), without removing of the native oxide layer, by thermal CVD using a precursor solution of 0.11 × 10^{-3} mol.L^{-1} of iron acetylacetonate ($Fe(acac)_3$) and 0.5 × 10^{-4} mol.L^{-1} of cobalt acetylacetonate ($Co(acac)_2$) in ethanol. A pressure of 15 mbar, a temperature of 400 °C and a gas flux of oxygen and argon with a ratio 1:1 with a total flow rate of 200 mL/min were identified as the optimal conditions for the growth of the crystalline CFO inverse spinel phase. Two injection rates of the precursor solution were employed in this study: 90 mL/h (growth rate of about 1.2 nm/min) and 30 mL/h (growth rate of about 0.4 nm/min). These growth conditions are hereafter referred to as CFO_90 and CFO_30, respectively.

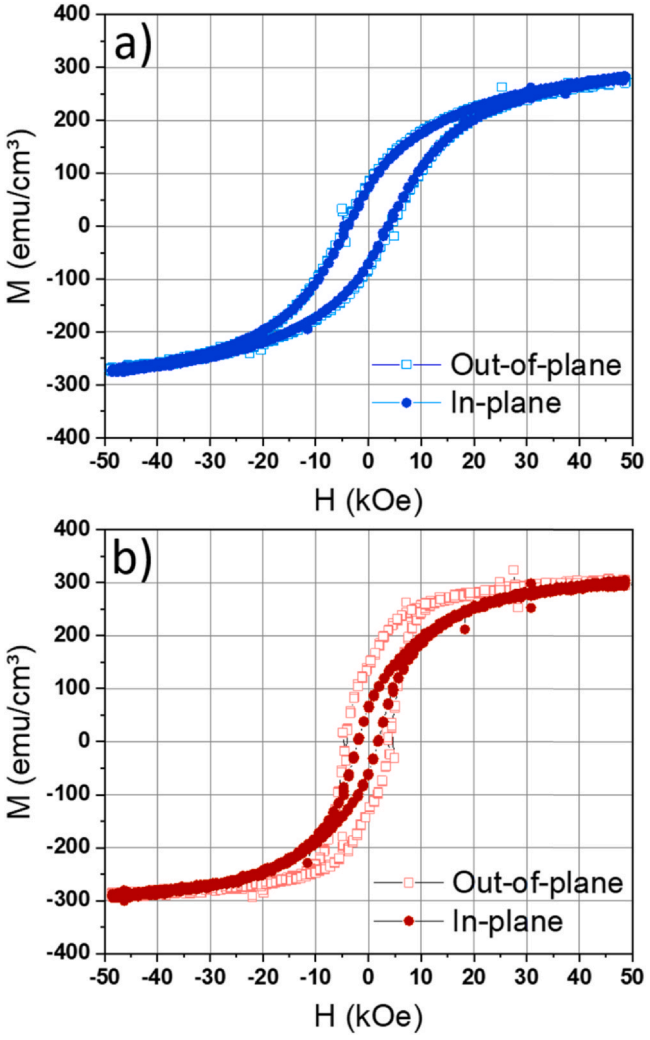

Fig. 4. In-plane and out-of-plane magnetization curves of (a) CFO_90 and (b) CFO_30.

X-ray diffraction analyses were performed in Bragg-Brentano geometry for diffraction angles between 20° to 50 ° using a Bruker D8 Advance, equipped with a Cu Kα X-ray source. Raman characterizations were performed at room temperature using an InVia Raman Spectrometer from Renishaw with a 532 nm laser used at the power of 8.5 mW. The films morphology and chemical compositions were investigated at 5 kV using a FEI Helios Nanolab 650 scanning electron microscope (SEM) coupled with an energy dispersive X-ray spectroscopy detector (EDXS). Cross-section SEM was implemented to inspect the grain structure and assess the film thickness. Magnetic characterization was performed at room temperature by vibrating sample magnetometry (VSM) between 50 kOe and − 50 kOe.

3. Results and discussion

3.1. CFO thin films

SEM surface and cross-section inspections were performed to assess the impact of the precursor feeding rate under the optimized growth conditions. The deposition time was adjusted under the CFO_90 and CFO_30 conditions to attain a thickness of 300 nm, and the corresponding morphologies are illustrated in Fig. 1. CFO_90 shows a granular morphology both in the surface and cross section views (Fig. 1a and b), and the resulting grains exhibit a tendency to agglomerate forming a porous structure. These growth conditions clearly favour the nucleation over the crystallite growth which is not surprizing for depositions with high partial pressure of the precursors. Inversing this tendency is therefore attempted by reducing the precursor feeding rate, and the resulting CFO_30 films exhibit a clear dominance of crystal growth over their nucleation. While the surface morphology shows faceted ~50 nm large crystallites (Fig. 1c), the cross-section view reveals a columnar structure in which the dense initial nucleation is dominated by the fast growth of some crystallites over others (Fig. 1d). A similar CFO columnar structure was recently reported using a strong applied magnetic field (up to 4 T) during the Pulsed Laser Deposition at a significantly higher temperature (680 °C) [35]. It is worth reminding that the morphology attained in Fig. 1 corresponds to thermal activation with no further assistance, which makes the upscaling more straightforward. The expected Co:Fe ratio of 1:2 corresponding to the $CoFe_2O_4$ spinel phase was evidenced by EDX analyses on the thin films.

Table 1
Magnetic parameters of CFO samples.

Sample	Magnetization plane	M_s (emu/cm^3)	M_r (emu/cm^3)	M_r/M_s (%)	H_c (kOe)
CFO_90	In-plane	290	75	26	4.5
	Out-of-plane	290	75	26	4.5
CFO_30	In-plane	300	65	22	2
	Out-of-plane	300	135	45	4

The XRD analysis, Fig. 2, reveals only peaks that can be attributed to the CFO spinel phase and indexed with the cubic symmetry (JCPDS file #04-006-4148, space group: *Fd*-3*m* (227), $a = 8.366$ Å [36]). The observed broad peaks for the CFO_90 conditions are in line with the presence of small crystallites. The X-ray reflexes of CFO_90 exhibit a relative intensity that is similar to the powder database XRD pattern, which indicates a polycrystalline nature of the film. In contrast, CFO_30 features a strong < 100 > preferential orientation. This result agrees with the observed SEM morphology of CFO_30 and a potential c-axis dominant growth. The orientation factor of the (400) peak was computed by the Lotgering method [37] by comparing the CFO_30 XRD peaks intensity to powder from the database. The obtained factor is equal to 0.67. This (100)-preferred orientation on (100) silicon substrates obtained by CVD differs from the usual (111)-preferred orientation obtained by PLD technique [17], [35]. It is worth mentioning that the large lattice mismatch (~23%) with a doubled unit cell of cubic (100)Si (JCPDS file #00-005-0565, space group: *Fd*-3*m* (227), $a = 5.430$ Å) is not favourable for an improved CFO films' texture. Moreover, considering the amorphous native oxide layer on the silicone substrate, the substrate is not likely

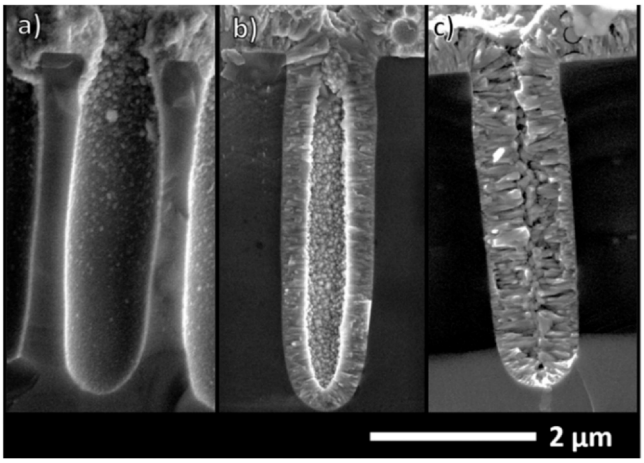

Fig. 5. Scanning electron micrographs of the cross-section of pores filling using a CFO precursor solution with (a) no H(acac), (b) 0.05×10^{-3} mol L^{-1} of H(acac), and (c) 0.1×10^{-3} mol L^{-1} of H(acac).

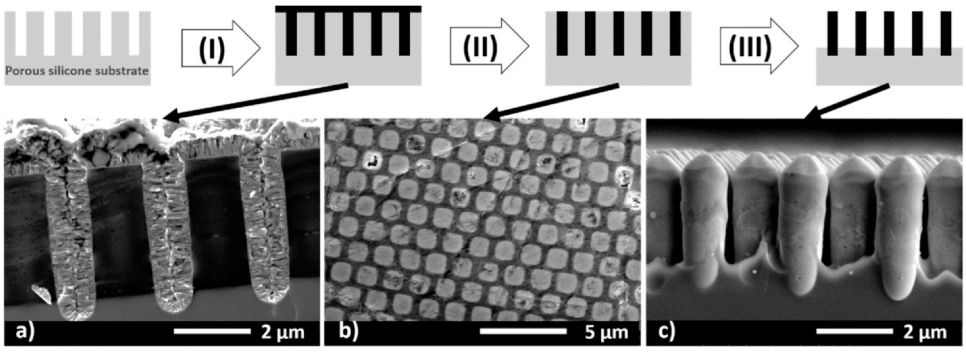

Fig. 6. Schematic description of the CFO pillar structure process visualized by scanning electron micrographs of (a) a cross-section after the CFO filling of the pores, (b) a top view after polishing, and (c) cross-section after reactive-ionic etching of the silicone substrate.

the main factor for the oriented growth. As observed at the interface region in Fig. 1d, the film presents a high nucleation density, but the further crystal growth is dominated by the (100) oriented among them. Therefore, the (100)-preferred orientation is driven by the minimization of the surface area and that of the total free energy with the interface and likely related to the growth temperature. In a recent study [15], authors used a two steps DC magnetron sputtering method to induce the growth of the (100) orientation in CFO. Authors noticed that the growth at room temperature yields a CFO layer that presents a maximal (100) orientation for a thickness of 8 nm. Further growth at a higher temperature, on the 8 nm oriented seed layer, yields a (100) oriented CFO growth [38]. Moreover, a study investigating the effect of the deposition temperatures of CFO in the PLD process showed an increase of the (400) orientation for temperatures around 450 °C compared to lower temperature [15]. In this work, although the CVD process operates in a single step and at a constant temperature, some similarities might be supposed. Conditions enabling a slow kinetics are favourable for the (100) CFO orientation, the surface diffusion favours the crystal growth over the nucleation of new ones. It is worth mentioning that the subtle ratio between nucleation and growth kinetics is temperature sensitive.

XRD stress measurements of the samples were performed on the (311) planes from $\psi = 0°$ to $\psi = 50°$. Leptos software was used to fit the peaks and assess the stress values. For both samples, similar strain values of 2.5% were retrieved. Those results were observed for $\varphi = 0°$ and $\varphi = 90°$. Approximate crystallite sizes were retrieved from the broadening of the XRD peaks. Values between 10 nm and 20 nm were obtained for CFO_90 whereas larger values between 40 nm and 70 nm were obtain for CFO_30. This result agrees with the larger crystallites of CFO_30 observed in Fig. 1. However, the inhomogeneity in crystallite sizes, visible on the SEM images, do not enable a precise estimation from the XRD patterns.

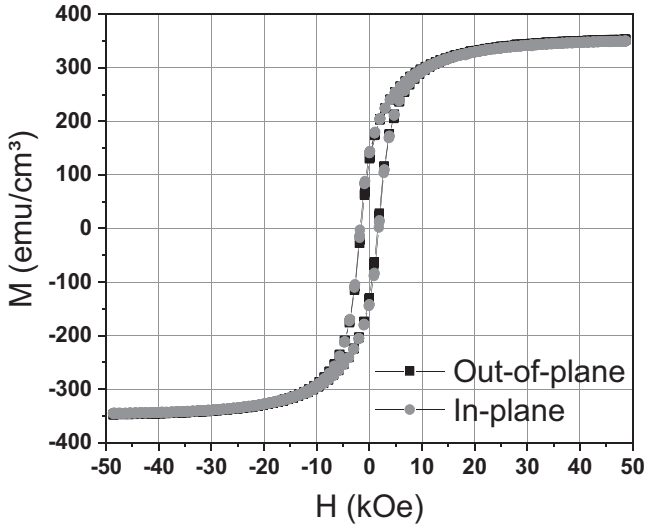

Fig. 7. In- and out-of-plane magnetization curves of CFO regular rod arrays.

The Raman spectra, Fig. 3, present the characteristic bands of CFO at 209, 306, 471, 573, 617 and 693 cm^{-1} [16,39]. Details of the phonon modes of the spinel structure have been investigated and described in the literature [40,41]. Out of the A_{1g} (R), E_g (R), T_{1g}, $3T_{2g}$ (R), $2A_{2u}$, $2E_u$, $4T_{1u}$ (IR) and $2T_{2u}$ phonon modes, five are Raman active (A_{1g}, E_g and $3T_{2g}$). The bands and phonon modes were assigned according to the literature [16,39,40]. Bands at 209, 306, 471 and 573 cm^{-1} are assigned to E_g and $3T_{2g}$ modes. CFO_90 and CFO_30 spectra exhibit peak maxima with an almost identical Raman shift. The slight shift can be attributed to the size of the grains [40] and to the occupation sites of the Co^{2+} cations [42]. An increase of the Raman intensity ratio of the 617 cm^{-1} and 469 cm^{-1} peaks would confirm that Co^{2+} shifts from the octahedral sites to the tetrahedral ones [43]. In this study, the difference between the ratios is not judged significant.

The magnetic hysteresis loops, for applied magnetic field in- and out- of plane, are presented in Fig. 4, and the extracted saturation magnetizations M_s, remanent magnetizations M_r and coercivities H_c are displayed in Table 1. It is worth mentioning that the saturation magnetization M_s refers to the value measured at an external field of 140 kOe and is estimated with a measurement error of about 5%. Contributions from the diamagnetic silicone substrates and the sample holder have been subtracted from the presented results.

The polycrystalline CFO thin film (CFO_90) features an in- and out-of-plane saturation magnetization of 290 emu/cm^3. A slight increase of both values was observed when adopting the conditions of CFO_30 associated with the (100) preferred orientation. Such an increase is generally observed in thin films upon post-deposition annealing [44–46], and is associated with the improved crystallisation [45–47]. The attained saturation magnetization for the as-deposited films in the conditions of CFO_30 is in the range of those reported for epitaxial CFO thin films [14,15] and epitaxially grown 1-µm-thick films [48], while the CFO bulk (prepared by CVD) yields a higher performance (~400 emu/cm^3) [49].

The coercivities presented in Table 1 are within the range of the reported values in the literature for CFO thin films, and the CFO_90 coercivity of 4.5 kOe is in the higher range of values reported [15,23,50]. The in-plane decrease of the coercivity of CFO_30 (to 2 kOe) is also generally observed in cobalt ferrite with the increase of the grain size [18,19], especially when exceeding the critical single domain size of ~40 nm [50,51].

CFO_30 magnetic characterizations reveal a magnetic anisotropy between the in-plane and out-of-plane properties compared to CFO_90 (as displayed in Fig. 4 and Table 1). Relative to the polycrystalline film, the (100) oriented CFO (CFO_30) exhibits a 2-fold

higher out-of-plane remanent magnetization and a 2-fold reduced in-plane coercivity. The out-of-plane coercivity and in-plane remanent magnetization remained virtually unchanged. This anisotropic behaviour can be correlated to the out-of-plane orientation of the crystallite growth and the < 100 > orientation in CFO films [17,25] as the [100] direction is reported as the easy magnetization direction in CFO single crystal [52].

3.2. One dimensional CFO structures

The integration of CFO into device architectures requires the optimization of the growth of various structures including ordered micropillar arrays. Toward the fabrication of multiferroic composite coatings, ferro/ferrimagnetic 1D geometries are promising as far as the strength of the magnetoelectric coupling is concerned [27–29,34]. The possibility to achieve conformal coatings with CVD is a considerable asset for the filling of structures, such as trenches, with high aspect ratios (AR = 3:1 – 10:1). Here, custom-made porous < 100 > silicone substrates were purchased from SmartMEMBRANES. The pores are 5 µm deep, feature a square shaped opening of $1 \times 1\ \mu m^2$ and display a hexagonal arrangement. The CFO_90 deposition conditions on these porous surfaces yield a film, whose cross-section morphology is displayed in Fig. 5a. A growth rate on the upper surface was estimated at 1.2 nm/min, whereas only 0.1 nm/min grew on the vertical walls of the pores. The observed one order of magnitude difference of the growth rate might be attributed to the fast dissociative-chemisorption and depletion of the precursors at the surface. This leads inherently to an obstruction of the opening with a marginal filling of the pores. One of the established approaches to circumvent this effect is to introduce a molecule that competes with the precursors for the highly accessible surface adsorption sites. This forces the precursors to diffuse further to sites with less competition, which enhances the growth conformality. The introduced molecule plays therefore the role of a growth inhibitor at the surface, and the optimization of its dosage in respect to the precursor is crucial. Such an approach was recently reported for the super-conformal growth of HfO_2 [53–55].

Acetylacetone, H(acac), was selected as the inhibitor and was added to the precursor solution. As the metallic precursors are metal acetylacetonates, the presence of acetylacetone is not expected to induce any alteration of the precursor chemistry and does not introduce additional elements that might contaminate the film.

Fig. 5 presents the filling profile of porous silicon using different concentrations of H(acac) in the precursor solution. Introducing 0.05×10^{-3} mol L^{-1} of H(acac) in the precursor solution yields a film, whose cross-section in displayed in Fig. 5b. The growth rate on the upper surface is significantly reduced, 0.3 nm/min instead of the initially observed 1.2 nm/min, which confirms the inhibitor character of this molecule. Although a substantial improvement is observed for the morphology, the complete filling was not achieved as a pinch-off effect leads to the clogging of the opening of the micropores. Increasing the concentration of the inhibitor to 0.1×10^{-3} mol L^{-1} yields a complete filling as depicted in Fig. 5c. It is worth mentioning that the resulting films present a columnar structure although the precursor feeding rate is representative for the conditions of CFO_90, where a granular morphology prevailed. This is attributed to the decreased deposition rate due to the addition of acetylacetone. Although the CFO_30 conditions lead to this morphology, the implementation of an inhibitor is required to obtain a conformal filling of the pores. Using these conditions, however, results in an excessively reduced growth rate. Therefore, when adding acetylacetone, the CFO_90 conditions were chosen instead to enable a conformal filling with a columnar growth at acceptable rate. The films inside the pores feature a growth orientation perpendicular to the walls (i.e., in the substrate plane). The grains are about 500 nm long and 50–150 nm wide.

Based on this optimization, the conditions of CFO_90 with the inhibitor concentration of 0.1×10^{-3} mol L^{-1} were implemented to fill the ordered micro-pores with CFO. The microfabrication was performed using the workflow schematically represented in Fig. 6. This includes **(I)** silicone pores filling, **(II)** mechanical polishing to remove the top CFO layer, and then **(III)** the CFO rods excavation along 2 h reactive-ion etching (RIE, Plasma-Therm, 790 SERIES) using CF_4 (95 sccm) and O_2 (5 sccm) at 30 mTorr and a plasma power of 200 W. SEM images of the samples after each step are displayed in Fig. 6. The erosion of the corners during the RIE process leads to rods with pyramidal tips. The excavated part of the pillar is about 3.4 µm high, whereas the base is $1 \times 1\ \mu m^2$ corresponding to an aspect ratio larger than 3:1. The composition of both the top and bottom parts of the rods, as measured by EDXS analysis, is similar and it corresponds to a Co:Fe ratio of 1:2. This observation confirms that both precursors diffuse efficiently along the micro-pores.

The magnetic hysteresis of the CFO rods following step III was measured for in- and out-of-plane applied fields, and the results are displayed in Fig. 7. A coercivity of ~1.8 kOe was observed for both in- and out-of-plane orientations. This coercivity is smaller relative to the obtained films, Table 1, and is within the range of those reported in the literature for nanoparticles [56]. Saturation magnetization values of 350 emu/cm^3 and remanent magnetization values of 130 emu/cm^3 were measured in- and out-of-plane. The micropillar arrays outperform the obtained films in terms of saturation magnetization and in terms of remanent magnetization, which is correlated to the larger formed crystallites. The obtained properties are similar to those reported for epitaxially grown CFO. The observed isotropy of the magnetic properties correlates with a decrease of the strain in the sample. Indeed, a strain of 0.2% was assessed by XRD, which is significantly low relative to the planar films (2.5%) despite of the columnar structure of the grains.

It is worth mentioning that the investigated rods feature a cylindrical shape composed of radially oriented long c-oriented crystallites. The cylindrical shape is expected to induce an out-of-plane magnetic shape anisotropy, whereas the radial c-oriented crystallites would induce an in-plane magneto-crystalline anisotropy. The competition between these anisotropic factors leads to an apparent isotropic magnetization behaviour. The expected temperature-sensitivity of the magneto-crystalline anisotropic contribution might enable adjusting the magnetic behaviour and triggering new applications of the CFO rod arrays.

4. Conclusion

Thermal CVD was optimized for the growth of $CoFe_2O_4$ at 400 °C using metal beta-diketonates as precursors. The use of acetylacetone as a growth inhibitor was investigated to enhance the conformal nature of the coating on structured surfaces and to attain an efficient micro-pores filling. A microfabrication routine was implemented to excavate CFO ordered micropillar arrays, whose magnetic properties outperform the ones of the film obtained using the same process. The resulting regular 1D structures are considered as an important milestone towards the development of magnetoelectric composite coatings with a strong coupling.

CRediT authorship contribution statement

B. Aspe: Methodology, Investigation, Data curation, Writing – original draft, Visualization. **A. Malyeyev:** Investigation. **A. Vakilinejad:** Investigation. **K. Menguelti:** Investigation. **A. Michels:** Methodology, Supervision, Project administration, Funding acquisition. **N. Bahlawane:** Conceptualization, Methodology, Data curation, Writing – review & editing, Supervision, Project administration, Funding acquisition.

Declaration of Competing Interest

The authors declare that they have no known competing financial interests or personal relationships that could have appeared to influence the work reported in this paper.

Acknowledgement

Authors would like to acknowledge funding through the CORE program of the Luxembourg National Research Fund (project ID: C17/MS/11661571; SANS4NCC).

Appendix A. Supporting information

Supplementary data associated with this article can be found in the online version at doi:10.1016/j.jallcom.2021.161758.

References

[1] S. Hirosawa, M. Nishino, S. Miyashita, Perspectives for high-performance permanent magnets: applications, coercivity, and new materials, Adv. Nat. Sci: Nanosci. Nanotechnol. 8 (1) (2017) 013002, https://doi.org/10.1088/2043-6254/aa597c
[2] J. Xie, M. Han, L. Chen, R. Kuang, L. Deng, Microwave-absorbing properties of NiCoZn spinel ferrites, J. Magn. Magn. Mater. 314 (1) (2007) 37–42, https://doi.org/10.1016/j.jmmm.2007.02.124
[3] A. Raveendran, M.T. Sebastian, S. Raman, Applications of microwave materials: a review, J. Electron. Mater. 48 (5) (2019) 2601–2634, https://doi.org/10.1007/s11664-019-07049-1
[4] E. Salahun, G. Tanne, P. Queffelec, P. Gelin, A.-L. Adenot, O. Acher Ferromagnetic composite-based and magnetically-tunable microwave devices, in: IEEE MTT-S International Microwave Symposium Digest (Cat. No.02CH37278), Seattle, WA, USA, 2002, 1185–1188. https://doi.org/10.1109/MWSYM.2002.1011862.
[5] D.C. Jiles, C.C.H. Lo, The role of new materials in the development of magnetic sensors and actuators, Sens. Actuators A Phys. 106 (1–3) (2003) 3–7, https://doi.org/10.1016/S0924-4247(03)00255-3
[6] B. Yoo, S.-M. Na, A.B. Flatau, D.J. Pines, Directional magnetostrictive patch transducer based on Galfenol's anisotropic magnetostriction feature, Smart Mater. Struct. 23 (9) (2014) 095035, https://doi.org/10.1088/0964-1726/23/9/095035
[7] J.A. Paulsen, A.P. Ring, C.C.H. Lo, J.E. Snyder, D.C. Jiles, Manganese-substituted cobalt ferrite magnetostrictive materials for magnetic stress sensor applications, J. Appl. Phys. 97 (2005) 044502, https://doi.org/10.1063/1.1839633
[8] H. Zhang, T. Zhang, C. Jiang, Magnetostrictive actuators with large displacement and fast response, Smart Mater. Struct. 21 (5) (2012) 055014, https://doi.org/10.1088/0964-1726/21/5/055014
[9] J. Wang, X. Gao, C. Yuan, J. Li, X. Bao, Magnetostriction properties of oriented polycrystalline $CoFe_2O_4$, J. Magn. Magn. Mater. 401 (2016) 662–666, https://doi.org/10.1016/j.jmmm.2015.10.073
[10] W.H. Wang, X. Ren, Flux growth of high-quality $CoFe_2O_4$ single crystals and their characterization, J. Cryst. Growth 289 (2) (2006) 605–608, https://doi.org/10.1016/j.jcrysgro.2005.11.115
[11] K. Maaz, A. Mumtaz, S.K. Hasanain, A. Ceylan, Synthesis and magnetic properties of cobalt ferrite ($CoFe_2O_4$) nanoparticles prepared by wet chemical route, J. Magn. Magn. Mater. 308 (2) (2007) 289–295, https://doi.org/10.1016/j.jmmm.2006.06.003
[12] R.M. Bozorth, E.F. Tilden, A.J. Williams, Anisotropy and magnetostriction of some ferrites, Phys. Rev. 99 (6) (1955) 1788–1798, https://doi.org/10.1103/PhysRev.99.1788
[13] T.E. Quickel, V.H. Le, T. Brezesinski, S.H. Tolbert, On the correlation between nanoscale structure and magnetic properties in ordered mesoporous cobalt ferrite ($CoFe_2O_4$) thin films, Nano Lett. 10 (8) (2010) 2982–2988, https://doi.org/10.1021/nl1014266
[14] F. Eskandari, S.B. Porter, M. Venkatesan, P. Kameli, K. Rode, J.M.D. Coey, Magnetization and anisotropy of cobalt ferrite thin films, Phys. Rev. Mater. 1 (7) (2017) 074413, https://doi.org/10.1103/PhysRevMaterials.1.074413
[15] A. Raghunathan, I.C. Nlebedim, D.C. Jiles, J.E. Snyder, Growth of crystalline cobalt ferrite thin films at lower temperatures using pulsed-laser deposition technique, J. Appl. Phys. 107 (2010) 09A516, https://doi.org/10.1063/1.3357315
[16] M. Oujja, L. Martín-García, E. Rebollar, A. Quesada, M.A. García, J.F. Fernández, J.F. Marco, J. de la Figuera, M. Castillejo, Effect of wavelength, deposition temperature and substrate type on cobalt ferrite thin films grown by pulsed laser deposition, Appl. Surf. Sci. 452 (2018) 19–31, https://doi.org/10.1016/j.apsusc.2018.05.012
[17] M.C. Terzzoli, S. Duhalde, S. Jacobo, L. Steren, C. Moina, High perpendicular coercive field of $CoFe_2O_4$ thin films deposited by PLD, J. Alloy. Compd. 369 (1–2) (2004) 209–212, https://doi.org/10.1016/j.jallcom.2003.09.086
[18] J.-G. Lee, K.P. Chae, J.C. Sur, Surface morphology and magnetic properties of $CoFe_2O_4$ thin films grown by a RF magnetron sputtering method, J. Magn. Magn. Mater. 267 (2) (2003) 161–167, https://doi.org/10.1016/S0304-8853(03)00348-2
[19] H. Onoda, H. Sukegawa, H. Yanagihara, Study of induced magnetic anisotropy by lattice distortion in cobalt ferrite thin film grown on $(Mg,Sn)_3O_4$ buffer layers, IEEE Trans. Magn. 56 (3) (2020) 1–4, https://doi.org/10.1109/TMAG.2019.2962025
[20] P.M. Kouotou, Z.-Y. Tian, Cobalt-iron oxides made by CVD for low temperature catalytic application: cobalt-iron oxides for low temperature catalytic application, Phys. Status Solid. A 212 (7) (2015) 1508–1513, https://doi.org/10.1002/pssa.201532299
[21] Z.-Y. Tian, P. Mountapmbeme Kouotou, A. El Kasmi, P.H. Tchoua Ngamou, K. Kohse-Höinghaus, H. Vieker, A. Beyer, A. Gölzhäuser, Low-temperature deep oxidation of olefins and DME over cobalt ferrite, Proc. Combust. Instig. 35 (2) (2015) 2207–2214, https://doi.org/10.1016/j.proci.2014.06.111
[22] G.A. Sawatzky, F. Van der Woude, A.H. Morrish, Cation distributions in octahedral and tetrahedral sites of the ferrimagnetic spinel $CoFe_2O_4$, J. Appl. Phys. 39 (2) (1968) 1204–1205, https://doi.org/10.1063/1.1656224
[23] Y.C. Wang, J. Ding, J.B. Yi, B.H. Liu, T. Yu, Z.X. Shen, High-coercivity Co-ferrite thin films on (100)-SiO_2 substrate, Appl. Phys. Lett. 84 (14) (2004) 2596–2598, https://doi.org/10.1063/1.1695438
[24] Y.Q. Dai, J.M. Dai, X.W. Tang, Z.F. Zi, K.J. Zhang, X.B. Zhu, J. Yang, Y.P. Suna, Magnetism of $CoFe_2O_4$ thin films annealed under the magnetic field, J. Magn. Magn. Mater. 394 (2015) 287–291, https://doi.org/10.1016/j.jmmm.2015.06.089
[25] W. Huang, J. Zhu, H.Z. Zeng, X.H. Wei, Y. Zhang, Y.R. Li, Strain induced magnetic anisotropy in highly epitaxial CoFe2O4 thin films, Appl. Phys. Lett. 89 (2006) 262506, https://doi.org/10.1063/1.2424444
[26] P. Yu, A.V. Sukhorukov, N.G. Telegin, A.P. Bebenin, V.D. Nosov, Bessonov, A.A. Buchkevich, Strain-magneto-optics of a magnetostrictive ferrimagnetic $CoFe_2O_4$, Solid State Commun. 263 (2017) 27–30, https://doi.org/10.1016/j.ssc.2017.07.003
[27] A. Chen, Z. Bi, Q. Jia, J.L. MacManus-Driscoll, H. Wang, Microstructure, vertical strain control and tunable functionalities in self-assembled, vertically aligned nanocomposite thin films, Acta Mater. 61 (8) (2013) 2783–2792, https://doi.org/10.1016/j.actamat.2012.09.072
[28] H. Zheng, Multiferroic $BaTiO_3$-$CoFe_2O_4$ nanostructures, Science 303 (5658) (2004) 661–663, https://doi.org/10.1126/science.1094207
[29] D.H. Kim, S. Ning, C.A. Ross, Self-assembled multiferroic perovskite–spinel nanocomposite thin films: epitaxial growth, templating and integration on silicon, J. Mater. Chem. C 7 (30) (2019) 9128–9148, https://doi.org/10.1039/C9TC02033K
[30] F. Zavaliche, T. Zhao, H. Zheng, F. Straub, M.P. Cruz, P.-L. Yang, D. Hao, R. Ramesh, Electrically assisted magnetic recording in multiferroic nanostructures, Nano Lett. 7 (6) (2007) 1586–1590, https://doi.org/10.1021/nl070465o
[31] K.-S. Chang, M.A. Aronova, C.-L. Lin, M. Murakami, M.-H. Yu, J. Hattrick-Simpers, O.O. Famodu, S.Y. Lee, R. Ramesh, M. Wuttig, I. Takeuchi, Exploration of artificial multiferroic thin-film heterostructures using composition spreads, Appl. Phys. Lett. 84 (16) (2004) 3091–3093, https://doi.org/10.1063/1.1699474
[32] L. Shen, M. Liu, C. Ma, L. Lu, H. Fu, C. You, X. Lu, Chun-Lin Jiaabe, Enhanced bending-tuned magnetic properties in epitaxial cobalt ferrite nanopillar arrays on flexible substrates, Mater. Horiz. 5 (2) (2018) 230–239, https://doi.org/10.1039/C7MH00939A
[33] G. Tian, F. Zhang, J. Yao, H. Fan, P. Li, Z. Li, X. Song, X. Zhang, M. Qin, M. Zeng, Z. Zhang, J. Yao, X. Gao, J. Liu, Magnetoelectric coupling in well-ordered epitaxial $BiFeO_3$/$CoFe_2O_4$/$SrRuO_3$ heterostructured nanodot array, ACS Nano 10 (1) (2016) 1025–1032, https://doi.org/10.1021/acsnano.5b06339
[34] J.L. MacManus-Driscoll, P. Zerrer, H. Wang, H. Yang, J. Yoon, A. Fouchet, R. Yu, M.G. Blamire, Q. Jia, Strain control and spontaneous phase ordering in vertical nanocomposite heteroepitaxial thin films, Nat. Mater. 7 (4) (2008) 314–320, https://doi.org/10.1038/nmat2124
[35] S. Zhu, X. Tang, R. Wei, L. Hu, X. Zuo, W. Song, J. Dai, X. Zhu, Y. Sun, Columnar $CoFe_2O_4$ thin films with improved magnetic properties via high magnetic field, J. Magn. Magn. Mater. 484 (2019) 95–99, https://doi.org/10.1016/j.jmmm.2019.04.009
[36] J. Teillet, F. Bouree, R. Krishnan, Magnetic structure of $CoFe_2O_4$, J. Magn. Magn. Mater. 123 (1–2) (1993) 93–96, https://doi.org/10.1016/0304-8853(93)90017-V
[37] F.K. Lotgering, Topotactical reactions with ferrimagnetic oxides having hexagonal crystal structures—I, J. Inorg. Nucl. Chem. 9 (2) (1959) 113–123, https://doi.org/10.1016/0022-1902(59)80070-1
[38] S.E. Shirsath, D. Wang, J. Zhang, A. Morisako, S. Li, X. Liu, Single-crystal-like textured growth of $CoFe_2O_4$ thin film on an amorphous substrate: a self-bilayer approach, ACS Appl. Electron. Mater. 2 (11) (2020) 3650–3657, https://doi.org/10.1021/acsaelm.0c00716
[39] P.R. Graves, C. Johnston, J.J. Campaniello, Raman scattering in spinel structure ferrites, Mater. Res. Bull. 23 (11) (1988) 1651–1660, https://doi.org/10.1016/0025-5408(88)90255-3
[40] P. Chandramohan, M.P. Srinivasan, S. Velmurugan, S.V. Narasimhan, Cation distribution and particle size effect on Raman spectrum of $CoFe_2O_4$, J. Solid State Chem. 184 (1) (2011) 89–96, https://doi.org/10.1016/j.jssc.2010.10.019
[41] M. Lazzeri, P. Thibaudeau, *Ab initio* Raman spectrum of the normal and disordered $MgAl_2O_4$ spinel, Phys. Rev. B 74 (14) (2006) 140301, https://doi.org/10.1103/PhysRevB.74.140301
[42] N. Bahlawane, P.H.T. Ngamou, V. Vannier, T. Kottke, J. Heberle, K. Kohse-Höinghaus, Tailoring the properties and the reactivity of the spinel cobalt oxide, Phys. Chem. Chem. Phys. 11 (40) (2009) 9224–9232, https://doi.org/10.1039/b910707j
[43] D. Sharma, N. Khare, Tuning of optical bandgap and magnetization of CoFe2O4 thin films, Appl. Phys. Lett. 105 (2014) 032404, https://doi.org/10.1063/1.4890863

[44] E. Swatsitang, S. Phokha, S. Hunpratub, B. Usher, A. Bootchanont, S. Maensiri, P. Chindaprasirta, Characterization and magnetic properties of cobalt ferrite nanoparticles, J. Alloy. Compd. 664 (2016) 792–797, https://doi.org/10.1016/j.jallcom.2015.12.230

[45] P. Laokul, S. Arthan, S. Maensiri, E. Swatsitang, Magnetic and optical properties of $CoFe_2O_4$ nanoparticles synthesized by reverse micelle microemulsion method, J. Supercond. Nov. Magn. 28 (8) (2015) 2483–2489, https://doi.org/10.1007/s10948-015-3068-8

[46] M. Sangmanee, S. Maensiri, Nanostructures and magnetic properties of cobalt ferrite ($CoFe_2O_4$) fabricated by electrospinning, Appl. Phys. A 97 (1) (2009) 167–177, https://doi.org/10.1007/s00339-009-5256-5

[47] Y. Chen, M. Ruan, Y.F. Jiang, S.G. Cheng, W. Li, The synthesis and thermal effect of $CoFe_2O_4$ nanoparticles, J. Alloy. Compd. 493 (1–2) (2010) 1–2, https://doi.org/10.1016/j.jallcom.2009.12.170

[48] L. Shen, M. Althammer, N. Pachauri, B. Loukya, R. Datta, M. Iliev, N. Bao, A. Gupta, Epitaxial growth of spinel cobalt ferrite films on $MgAl_2O_4$ substrates by direct liquid injection chemical vapor deposition, J. Cryst. Growth 390 (2014) 61–66, https://doi.org/10.1016/j.jcrysgro.2013.12.012

[49] Y. Suzuki, G. Hu, R.B. van Dover, R.J. Cava, Magnetic anisotropy of epitaxial cobalt ferrite thin films, J. Magn. Magn. Mater. 191 (1–2) (1999) 1–8, https://doi.org/10.1016/S0304-8853(98)00364-3

[50] X. Tang, L. Jin, R. Wei, X. Zhu, J. Yang, J. Dai, W. Song, X. Zhu, Y. Sun, High-coercivity $CoFe_2O_4$ thin films on Si substrates by sol-gel, J. Magn. Magn. Mater. 422 (2017) 255–261, https://doi.org/10.1016/j.jmmm.2016.09.022

[51] N.S. Gajbhiye, S. Prasad, G. Blaji, Experimental study of Hopkinson effect in single domain $CoFe_2O_4$ particles, IEEE Trans. Magn. 35 (4) (1999) 2155–2161, https://doi.org/10.1109/20.774187

[52] M. Guillot, J. Ostorero, A. Marchand, High magnetic field magnetization study in cadmium-cobalt ferrite single crystals, Z. Phys. B Condens. Matter 71 (2) (1988) 193–197, https://doi.org/10.1007/BF01312789

[53] T.K. Talukdar, W.B. Wang, G.S. Girolami, J.R. Abelson, Superconformal coating and filling of deep trenches by chemical vapor deposition with forward-directed fluxes, J. Vac. Sci. Technol. A 36 (5) (2018) 051513, https://doi.org/10.1116/1.5038100

[54] T.K. Talukdar, G.S. Girolami, J.R. Abelson, Seamless fill of deep trenches by chemical vapor deposition: use of a molecular growth inhibitor to eliminate pinch-off, J. Vac. Sci. Technol. A 37 (2) (2019) 021509, https://doi.org/10.1116/1.5068684

[55] J.R. Abelson, G.S. Girolami, New strategies for conformal, superconformal, and ultrasmooth films by low temperature chemical vapor deposition, J. Vac. Sci. Technol. A 38 (3) (2020) 030802, https://doi.org/10.1116/6.0000035

[56] D. Zhao, X. Wu, H. Guan, E. Han, Study on supercritical hydrothermal synthesis of $CoFe_2O_4$ nanoparticles, J. Supercrit. Fluids 42 (2) (2007) 226–233, https://doi.org/10.1016/j.supflu.2007.03.004